

Miniband effect on optical vibrations in short-period $\text{In}_x\text{Ga}_{1-x}\text{As}/\text{InP}$ superlattices

Yu. A. Pusep

Instituto de Física de São Carlos, Universidade de São Paulo, 13560-970 São Carlos, SP, Brazil

A. de Giovanni Rodrigues and J. C. Galzerani

Departamento de Física, Universidade Federal de São Carlos, CP 676, 13565-905 São Carlos, SP, Brazil

D. M. Cornet, D. Comedi, and R. R. LaPierre

Centre for Emerging Device Technologies, McMaster University, Hamilton, Ontario, Canada L8S 4L7

(Received 27 January 2006; revised manuscript received 31 March 2006; published 26 June 2006)

The formation of the miniband electron energy structure and its effect on optical vibrational modes were explored in doped $\text{In}_x\text{Ga}_{1-x}\text{As}/\text{InP}$ superlattices with different periods. The analysis of the high resolution x-ray diffraction, Raman and magnetotransport data allowed us to conclude that in spite of the defect structure of the layers constituting the superlattices, their superperiodicity was well defined. The blueshift of the coupled plasmon-LO phonon modes was observed with decreasing superlattice period consistent with the development of the minibands. The coherence lengths of the coupled modes were found to be considerably longer than those of the optical phonons. This provided a quantitative proof of the conditions for breakdown of the Raman selection rules. Due to the defect structure of the layers no Raman selection rules were observed for the longitudinal optical phonons in long-period superlattices. In contrast, the selection rules of the coupled plasmon-longitudinal optical phonon vibrations observed in short-period superlattices were demonstrated to occur due to the increase of the coherence lengths of the coupled modes with respect to the coherence lengths of the optical phonons.

DOI: [10.1103/PhysRevB.73.235344](https://doi.org/10.1103/PhysRevB.73.235344)

PACS number(s): 73.20.Mf, 78.30.Fs, 78.66.Fd

I. INTRODUCTION

$\text{In}_x\text{Ga}_{1-x}\text{As}/\text{InP}$ heterostructures present an important class of semiconductor materials with applications in infrared optoelectronics. Moreover, a large g factor found in these materials¹ makes them promising in the field of spintronics and quantum information processing. A manipulation of the electronic properties (including g -factor engineering) important in device applications is possible in superlattices (SLs)—structures consisting of periodic sequences of the layers made of two different semiconductor materials. In such structures the dynamic electron properties can be tuned in the direction perpendicular to the layers by a variation of their thicknesses or compositions. However, to the best of our knowledge evidence of the formation of the superlattice band structure in $\text{In}_x\text{Ga}_{1-x}\text{As}/\text{InP}$ SLs has been obtained only recently by high-field magnetotransport measurements.² The photoluminescence data presented in Ref. 2 also indicated the existence of the minibands which result from the SL periodicity.³ In Ref. 2 no effects of the miniband dispersion were detected in long-period SLs with the narrow minibands (with the width of a few meV).

In this paper we present an extensive investigation of doped $\text{In}_x\text{Ga}_{1-x}\text{As}/\text{InP}$ SLs with different periods by x-ray diffraction, Raman scattering and high-field magnetoresistance. The miniband widths of these SLs varied in the interval from 250 meV to the flat isolated electron levels. Therefore, the effects of the miniband dispersion were possible to distinguish. We explored the Raman scattering by the coupled plasmon-LO phonon modes propagating perpendicular to the layers of the $\text{In}_x\text{Ga}_{1-x}\text{As}/\text{InP}$ SLs. Such modes emerge due to the coupling between the longitudinal optical (LO) lattice vibrations and the collective electron excitations

(plasmons) resulting in significant blueshifts of the frequencies of the LO modes. We found no evidence of such modes in the long-period SLs. The manifestation of the coupled modes in the short-period SLs was assigned to the formation of the miniband energy structure caused by the SL periodicity. It should be mentioned that the effects of the plasmon-LO phonon coupling on the Raman scattering of doped $\text{In}_x\text{Ga}_{1-x}\text{As}/\text{InP}$ single quantum wells has been discussed in Refs. 4 and 5. We also found an additional indication of the miniband formation by high-magnetic field magnetoresistance measurements. Moreover, a considerable effect of the superperiodicity on the Raman selection rules of the coupled modes was observed: the longitudinal lattice vibrations detected in the long-period superlattices did not reveal any selection rules because of the defect structure of the bulk InGaAs and InP layers, while the coupled plasmon-LO phonon modes showed evidence in the superlattices of the expected Raman selection rules. Our data reveal that these selection rules came out due to the increase of the spatial coherence length of the coupled vibrations. These results provide additional evidence for the modification of the Raman selection rules induced by atomic-scale roughness in semiconductor SLs.⁶

II. EXPERIMENTAL

A total number of 30 periods of the lattice-matched $(\text{In}_{0.53}\text{Ga}_{0.47}\text{As})_m(\text{InP})_m$ SLs with $m=6, 7, 10, 15,$ and 68 ML (except the SL with $m=68$ which had 20 periods), where n is the thickness of the layers expressed in monolayers (1 ML = 2.9 Å), were grown on semi-insulating (001) InP substrates by molecular beam epitaxy. The barriers of the SLs were

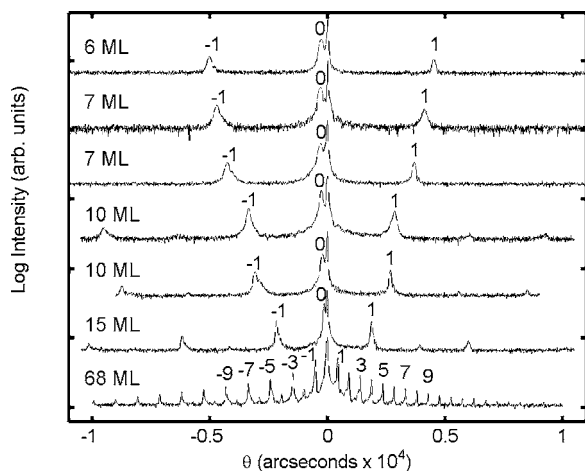


FIG. 1. Measured HRXRD (004) rocking curves. Nominal thicknesses of the well and barrier layers were identical and are indicated for each rocking curve. Curves are shown offset for clarity.

doped by Si in order to form a gas of degenerate electrons with the density $5.0 \times 10^{17} \text{ cm}^{-3}$. The doping was kept the same for all the reported SLs.

The SLs were characterized by high-resolution x-ray diffraction (HRXRD) rocking curves of the (004) reflection using the Bede D1 system. Each SL structure was determined by comparing the measured rocking curves to simulated curves to determine the degree of interface roughness and variation in SL periodicity. The simulated curves were obtained by using the Bede RADS Mercury (version 3.88) x-ray rocking curve software⁷ based on the Takagi-Taupin equations of dynamical diffraction theory.

The magnetoresistance measurements were performed on samples patterned into an active area of $4 \times 4 \text{ mm}$. The Ohmic contacts were fabricated by depositing indium. The transport measurements parallel to the surface of the samples were carried out at $T=4.2 \text{ K}$ in the Van der Pauw geometry using a standard low-frequency (5 Hz) lock-in technique in a liquid He cryostat with the magnetic fields directed perpendicular to the current. The Raman scattering was collected from the surface of the samples at $T=10 \text{ K}$ in the backscattering configuration with an “Instruments S.A. T64000” triple grating spectrometer supplied with a CCD detector cooled by liquid nitrogen. The 5145 Å line of an Ar⁺ laser was used for nonresonant excitation.

III. RESULTS AND DISCUSSION

The HRXRD rocking curves of the SLs are shown in Fig. 1, which exhibit the usual satellite peaks (order $\pm 1, \pm 2, \dots$) centered around the average composition peak (order 0). In terms of the consistency in the period of the SLs, the quality is quite good. This is apparent from the small amount of satellite peak broadening that occurs with satellite order. The uniformity of the satellite peak full width at half-maximum (FWHM) within each sample can be seen in Fig. 1, especially in the $m=68 \text{ ML}$ sample. A quantitative analysis of the peak broadening of the 68 ML sample shows that the FWHM

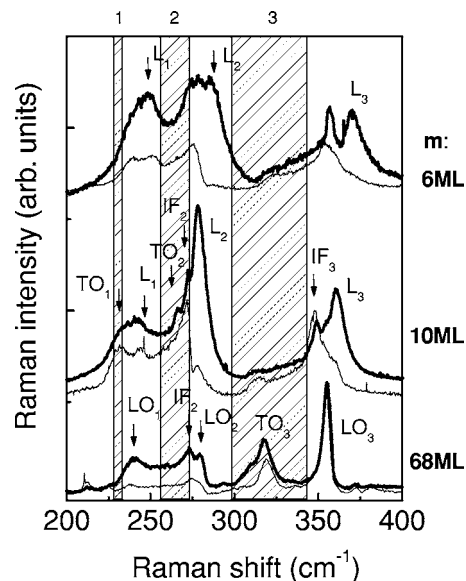


FIG. 2. Raman scattering measured at $T=10 \text{ K}$ in the $(\text{InGaAs})_m(\text{InP})_m$ superlattices with different periods. Thick and thin lines correspond to $z(x'y')\bar{z}$ and $z(x'x')\bar{z}$ scattering configurations, respectively. Shaded areas demonstrate the InAs-like (1), GaAs-like (2) and InP (3) “restrahlen” bands determined by the room temperature frequencies of the corresponding TO and LO phonons, available from the literature (Refs. 11 and 12).

of the satellite peaks increased by only about 1.5 arcseconds with each consecutive order. Clear broadening with increasing satellite order is a sign of significant variation in the SL period.⁸ When compared to data from other studies⁹ the variation in the period of our SLs can be estimated at about 0.3%. Excess broadening of each SL peak in comparison to the simulated peak widths (not shown) was consistent with an interface roughness of approximately 2 MLs.

The Raman spectra of the optical vibrational modes propagating along the growth direction measured in $z(x'y')\bar{z}$ cross- and $z(x'x')\bar{z}$ parallel-polarized configurations of the backscattering, where x', y', z are the crystallographic directions $[110], [1\bar{1}0],$ and $[001]$, respectively, are shown for selected SLs in Fig. 2. In such a case, according to the Raman selection rules derived for the deformation-potential electron-phonon interaction (the Fröhlich interaction gives vanishing contribution at the zone center, which is negligible in nonresonant conditions), the longitudinal optical lattice vibrations (LO) are active in the cross-polarized configuration, while no optical modes contribute to the parallel-polarized Raman scattering.¹⁰ For comparison, InAs-like (1), GaAs-like (2), and InP-like (3) “restrahlen” bands determined by experimental room temperature frequencies of the corresponding TO and LO phonons, available from the literature^{11,12} are also shown in Fig. 2 as shaded areas. As can be seen in this figure, we observe the following vibrational modes for the long-period $\text{In}_x\text{Ga}_{1-x}\text{As}/\text{InP}$ SL with both layers’ thicknesses equal to 68 ML: the allowed LO and the forbidden transverse optical (TO) vibration modes of the InGaAs wells (the InAs-like modes with the indices 1 and the GaAs-like modes with the indices 2, respectively) and the InP barriers (the modes with the indices 3). Moreover, the

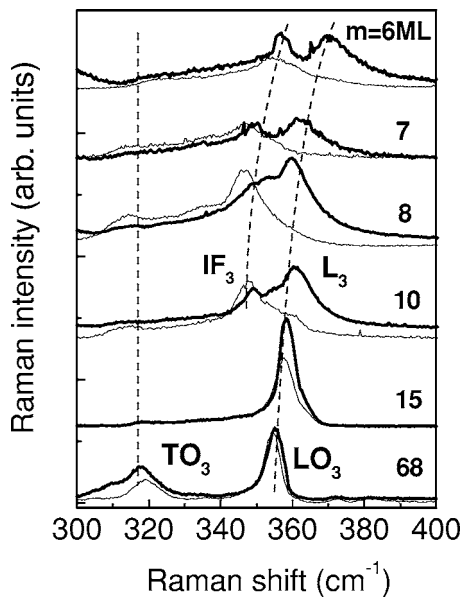


FIG. 3. Raman scattering measured at $T=10$ K in the $(\text{InGaAs})_m(\text{InP})_m$ superlattices with different periods in the range of InP lattice vibrations at $T=10$ K. Thick and thin lines correspond to $z(x'y')\bar{z}$ and $z(x'x')\bar{z}$ scattering configurations, respectively. The dashed lines indicate the positions of the corresponding Raman lines.

mode at 274 cm^{-1} may be identified as the GaAs-like interface (IF_2) disorder activated mode. No selection rules were found in this SL. The absence of the Raman selection rules and the evidence of the forbidden TO and IF modes are manifestations of the significant violation of the translational symmetry in the bulk materials constituting the SL. Also, the higher than expected temperature shifts of the InP modes may be caused by a modification of the structure of the InP barriers. At the same time, the expected Raman selection rules emerge when decreasing the period of the SLs and they are clearly determined in the SLs with the shortest periods ($m=6$ ML and 8 ML) for the longitudinal modes denoted as L_1 , L_2 , and L_3 . Besides, considerable blueshifts of these longitudinal modes were found with decreasing SL period. The behavior of the Raman lines measured in the range of the InP lattice vibrations in the $\text{In}_x\text{Ga}_{1-x}\text{As}/\text{InP}$ SL with different periods is depicted in Fig. 3 where both the emergence of the Raman selection rules for the longitudinal modes and their blueshifts are clearly seen, while the Raman lines corresponding to the transverse optical phonon of InP (TO_3) were found to remain unchanged with the variation of the period. The InP-like interface modes (IF_3) detected in the short-period SLs at 350 cm^{-1} also reveal a similar blueshift, which indicates their mostly longitudinal character.

The observed effects can be caused by a formation of the miniband structure in the electron energy spectrum of the SLs due to the superperiodicity. The dynamic properties of the electrons propagating in the growth direction of a SL are determined by the miniband dispersion $E(k_z)$, where k_z is the wave number along the growth direction z . With decreasing period the miniband dispersion increases and as a consequence, the effective mass of the electrons propagating in the

z direction (m_z) decreases resulting in the increase of the frequency of the plasmon oscillations polarized in the same direction according to $\omega_{pz} = (4\pi e^2 n / \epsilon_\infty m_z)^{1/2}$, where n is the electron concentration and ϵ_∞ is the dielectric constant of the superlattice. The coupling between the plasmons and the optical phonons with the same polarization causes the blueshift of the longitudinal modes observed in Figs. 2 and 3 and this shift increases with increasing plasmon frequency. The variation of the effective mass is responsible for the observed blueshift when the electron concentration is fixed. In such a case, the blueshift of the coupled plasmon-LO phonon modes can serve as a manifestation of the formation of the miniband energy structure.

In order to prove the effect of the miniband dispersion on the shift of the coupled modes we calculated the miniband effective mass in all the SLs. The calculations were performed using the envelope function approximation¹³ as in Ref. 14 with the band parameters taken from Ref. 15. The frequencies of the coupled plasmon-LO phonon modes were calculated as zeros of the corresponding diagonal component of the dielectric function tensor of a SL in the long wavelength approximation according to Ref. 16:

$$\epsilon_z(\omega) = \frac{d_1 + d_2}{d_1/\epsilon_1(\omega) + d_2/\epsilon_2(\omega)} - \frac{\omega_{pz}^2}{\omega^2} \quad (1)$$

with the dielectric function of the InGaAs layers determined as

$$\epsilon_1(\omega) = \epsilon_{\infty 1} \left(\frac{\omega_{L1}^2 - \omega^2}{\omega_{T1}^2 - \omega^2} + \frac{\omega_{L2}^2 - \omega^2}{\omega_{T2}^2 - \omega^2} \right) \quad (2)$$

and the dielectric function of the InP layers determined as

$$\epsilon_2(\omega) = \epsilon_{\infty 2} \left(\frac{\omega_{L3}^2 - \omega^2}{\omega_{T3}^2 - \omega^2} \right), \quad (3)$$

where d_1 and d_2 are the thicknesses of the corresponding layers, $\epsilon_{\infty 1}$ and $\epsilon_{\infty 2}$ are the dielectric constants of the InGaAs and InP, respectively, and ω_{Ln} and ω_{Tn} are the frequencies of the corresponding longitudinal and transverse phonons.

According to Eqs. (1)–(3) the spectrum of the longitudinal optical vibrations of the doped $\text{In}_x\text{Ga}_{1-x}\text{As}/\text{InP}$ SL consists of four modes: the low-frequency plasmonlike coupled L^- mode, the InAs-like coupled L_1 mode, the GaAs-like coupled L_2 mode and the InP-like coupled L_3 mode. Their dependence on the plasma frequency is shown in Fig. 4. All of these modes were found in the Raman spectra of the short-period $\text{In}_x\text{Ga}_{1-x}\text{As}/\text{InP}$ SLs except the low-frequency L^- mode, which is difficult to detect due to its low frequency. The hatched area of Fig. 4 indicates the region (the mode frequencies and the wave number expansion) where these modes were observed. It follows from the data presented in Fig. 4 that the L_1 and L_2 modes reveal no significant shift in the observed region. Moreover, these modes comprise the complex mixed character and they are hindered by the contributions of the TO and IF vibrations. Besides, the energy of the L_2 mode is affected by the spatial quantization of the GaAs-like phonons in the wells, while the effect of the quantization of the InP-like L_3 mode is insignificant due to the weak dispersion of the corresponding LO phonons. There-

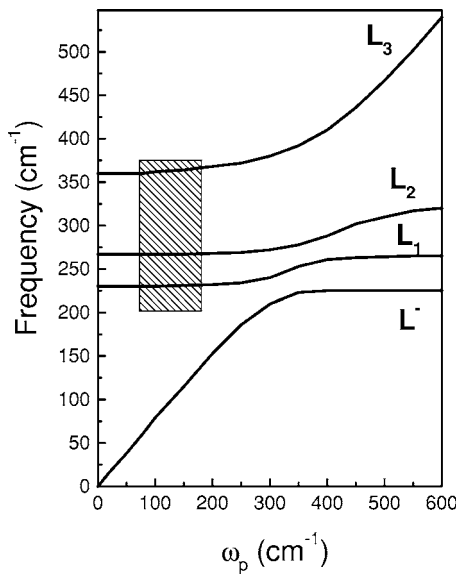


FIG. 4. Dependence of the frequencies of the coupled plasmon-LO phonon modes on the plasmon frequency calculated in the $(\text{InGaAs})_m(\text{InP})_m$ superlattice. The hatched area shows the region relevant to the superlattices studied here.

fore, we have concentrated our analysis on the behavior of the high-frequency L_3 coupled mode.

The calculated frequency shift of the InP-like coupled mode (L_3) together with the experimental data are shown in Fig. 5. A good agreement between the experimental and calculated results presented in Fig. 5 confirms that the observed blueshifts of the longitudinal modes are observed due to the miniband effect.

In addition, the miniband effect explains the emergence of the Raman selection rules observed for the coupled modes in the short-period SLs. As seen in Figs. 2 and 3 no selection rules expected for the longitudinal lattice modes were found in the long-period SLs, probably due to the defect structure of the constituent bulk materials. However, according to our data, the longitudinal lattice vibrations transform to the coupled plasmon-LO phonon modes in the short-period SLs. The coupled modes usually reveal the Raman selection rules of the LO phonons¹⁰ as indeed observed in the short-period SLs studied here. Raman scattering by the lattice vibrations exhibits corresponding selection rules when their spatial coherence length is significantly larger than the size of the crystal unit cell. We suppose that the coherence lengths of the optical phonons relevant to the SLs reported here are short enough to cause the breakdown of the Raman selection rules.¹⁷ At the same time, in the short-period SLs, the observed miniband effect indicates that the electrons propagate over several periods. Therefore, their collective excitations (plasmons), because of their coupling to the LO phonons, lead to an increase of the coherence length of the coupled vibrations. The Raman selection rules are probably a consequence of this enhancement of the coherence length.

In order to confirm the effect of the increase of the coherence length of the coupled plasmonlike vibrations on their Raman selection rules we determined and compared the coherence lengths of the optical phonons and of the coupled

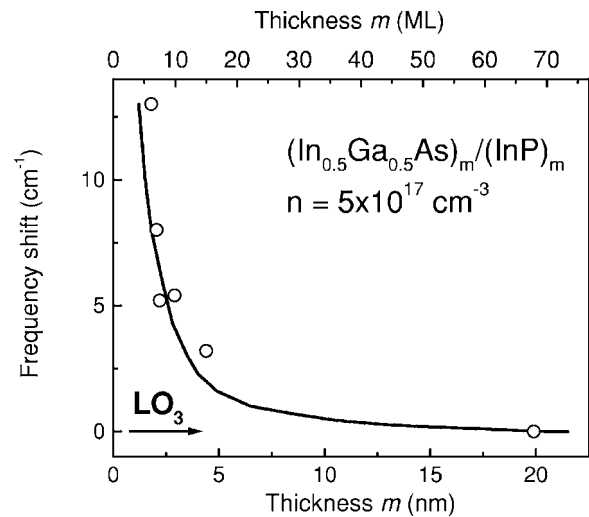


FIG. 5. Calculated (full line) and measured (open circles) frequency shifts of the InP coupled mode (L_3) relative to the frequency of the InP phonon (LO_3) measured in the $(\text{InGaAs})_m(\text{InP})_m$ superlattice with different layer thicknesses (m) and the same doping.

plasmon-LO phonon modes. As demonstrated in Ref. 18, in the presence of disorder a finite coherence length of the excitations involved in Raman scattering leads to the asymmetric Raman line shapes, which are distinctly different for the optical phonons and the coupled plasmonlike modes. Then, the shape of the Raman lines reproduces the density of states of the excitations that contribute to Raman scattering. In such a case, the coherence length of the relevant excitations may be obtained. We found the well pronounced asymmetries of the Raman lines of the LO_3 phonon of InP in the long-period SL ($m=68$ ML) and of the L_3 coupled mode in the short-period SL ($m=6$ ML). The asymmetries of the phonon and the coupled lines are different due to their different dispersions [shown in Figs. 6(a) and 6(b)]. The fitting of the Raman intensities calculated as in Ref. 18 to the experimental spectra shown in Figs. 6(c) and 6(d) allowed us to determine the corresponding coherence lengths (L_c): 0.5 nm and 12 nm for the InP longitudinal optical phonon and for the coupled L_3 mode, respectively. Obviously, the obtained phonon coherence length is of the order of the crystal unit cell size and, therefore, the phonon Raman lines did not reveal the selection rules. In contrast, the much stronger coherence of the plasmon-LO phonon modes resulted in their symmetrical properties determined by the crystal lattice and, as a consequence, in the corresponding selection rules. The dispersions of the excitations analyzed above, which are indispensable for the calculations of the Raman intensities are shown in Figs. 6(a) and 6(b). The dispersion of the coupled mode was calculated in the random phase approximation, while the dispersion of the InP LO phonon was taken from Ref. 12.

Finally, an additional confirmation of the formation of the miniband energy structure was obtained by the high-field magnetoresistance measurements. The Shubnikov-de Haas oscillations measured with different orientations of the magnetic field (Fig. 7) demonstrate a formation of the quantized Landau levels and show a well pronounced anisotropy of the

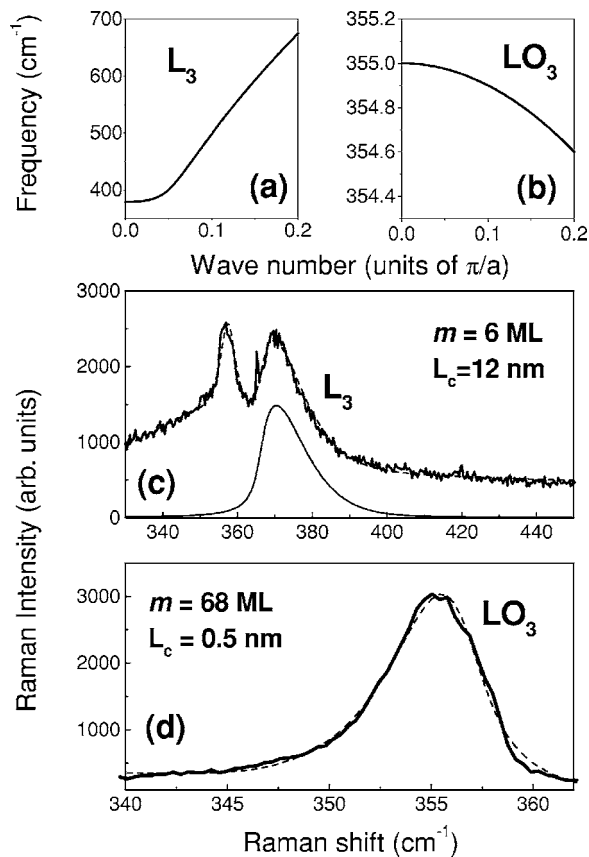


FIG. 6. Dispersion of the coupled L_3 mode calculated in the superlattice with $m=6$ ML (a) and the dispersion of the LO_3 phonons in InP (b). The Raman intensities measured in the range of the InP optical vibrations: (c) in the superlattice with $m=6$ ML and (d) in the superlattice with $m=68$ ML. The dashed lines were calculated as in Ref. 18. The contribution of the coupled L_3 mode is shown in (c) by the thin line.

magnetoresistance as expected in SLs due to the different parallel and vertical effective masses. The fitting of the magnetoresistances calculated according to Ref. 19 to the experimental magnetoresistance traces allowed us to obtain the Fermi energies, the vertical effective masses (m_{\perp}) and the ratios of the parallel to vertical relaxation times ($\tau_{\parallel}/\tau_{\perp}$) shown in Figs. 7(a) and 7(b). The calculations were performed with the parallel effective mass of $0.05m_0$ corresponding to $\text{In}_{0.53}\text{Ga}_{0.47}\text{As}$.¹⁵ The difference found between the parallel and vertical effective masses once again reveals the effect of the formation of the superlattice miniband.

IV. CONCLUSION

Doped $\text{In}_x\text{Ga}_{1-x}\text{As}/\text{InP}$ SLs with different periods were explored by x-ray diffraction, Raman scattering and high-

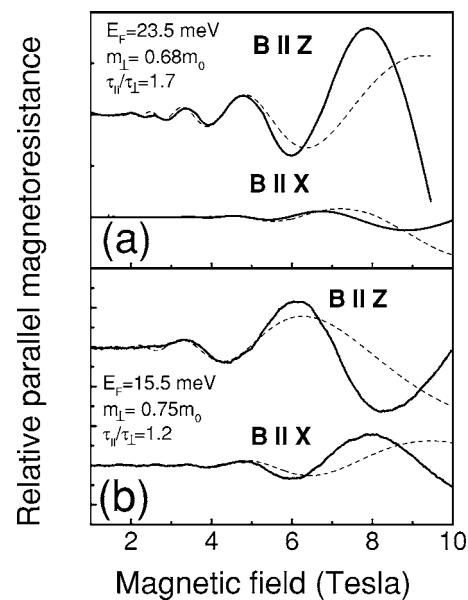


FIG. 7. Oscillatory parts of the high-field magnetoresistances (solid lines) measured with different orientations of the magnetic field at $T=4.2$ K in the $(\text{InGaAs})_m(\text{InP})_m$ superlattices with different periods: (a) $m=6$ ML, (b) $m=15$ ML. Dashed lines show the corresponding calculated magnetoresistances.

field magnetoresistance measurements. Clear evidence of the formation of the miniband structure in the electron energy spectrum was observed. No Raman selection rules were detected for the LO phonon modes in the long-period $\text{In}_x\text{Ga}_{1-x}\text{As}/\text{InP}$ SLs, while the distinct selection rules were found for the coupled plasmon-LO phonon modes propagating in the growth direction of the short-period SLs. We demonstrated that the selection rules of the coupled modes appear due to the increase of their coherence length. The analysis of the diffraction and Raman data allowed us to conclude that in spite of the defect structure of the layers constituting the SLs, their superperiodicity was well determined. The magnetoresistance measured in the $\text{In}_x\text{Ga}_{1-x}\text{As}/\text{InP}$ SLs also demonstrated the anisotropy of the miniband effective electron mass due to the formation of the miniband structure.

ACKNOWLEDGMENTS

The authors are grateful to H. Arakaki and C.A. de Souza for technical assistance. The financial support from Brazilian agencies FAPESP, CNPq and the Natural Sciences and Engineering Research Council of Canada is gratefully acknowledged.

- ¹C. Hermann and C. Wesbuch, *Phys. Rev. B* **15**, 823 (1977).
- ²A. B. Henriques, L. K. Hanamoto, R. F. Oliveira, P. L. Souza, L. C. D. Gonçalves, and B. Yavich, *Braz. J. Phys.* **29**, 707 (1999).
- ³C. Weisbuch and B. Vinter, *Quantum Semiconductor Structures: Fundamentals and Applications*, (Academic, San Diego, 1991).
- ⁴D. J. Mowbray, W. Hayes, J. A. C. Bland, M. S. Skolnick, and S. J. Bass, *Semicond. Sci. Technol.* **2**, 822 (1987).
- ⁵D. J. Mowbray, W. Hayes, L. L. Taylor, and S. J. Bass, *Semicond. Sci. Technol.* **5**, 83 (1989).
- ⁶Yu. A. Pusep, S. W. da Silva, J. C. Galzerani, D. I. Lubyshev, and P. Basmaji, *Phys. Rev. B* **51**, 9891 (1995).
- ⁷Bede Scientific Instruments Ltd., Bowburn South Industrial Estate, Bowburn, Durham, England.
- ⁸W. J. Bartels, in *Thin-Film Growth Techniques for Low-Dimensional Structures*, Vol. 163 of NATO Advanced Study Institute, Series B: Physics, edited by R. F. C. Farrow and P. J. Dobson (Plenum, New York, 1987), p. 441.
- ⁹W. J. Bartels, J. Hornstra, and D. J. W. Lobeek, *Acta Crystallogr., Sect. A: Found. Crystallogr.* **A42**, 539 (1986).
- ¹⁰*Light Scattering in Solids V*, edited by M. Cardona and G. Güntherodt (Springer-Verlag, Berlin, 1989).
- ¹¹M. H. Brodsky and G. Lucovsky, *Phys. Rev. Lett.* **21**, 990 (1968).
- ¹²*Landolt-Börnstein Series*, edited by O. Madelung (Springer-Verlag, Berlin, 1982), Vol. 17.
- ¹³G. Bastard, *Phys. Rev. B* **24**, 5693 (1981).
- ¹⁴Yu. A. Pusep, A. G. Milekhin, N. T. Moshegov, and A. I. Toropov, *J. Phys.: Condens. Matter* **6**, 93 (1994).
- ¹⁵I. Vurgaftman, J. R. Meyer, and L. R. Ram-Mohan, *J. Appl. Phys.* **89**, 5815 (2001).
- ¹⁶Yu. Pusep, A. Milekhin, and A. Toropov, *Superlattices Microstruct.* **13**, 115 (1993).
- ¹⁷R. Shuker and R. W. Gammon, *Phys. Rev. Lett.* **25**, 222 (1970).
- ¹⁸Yu. A. Pusep, M. T. O. Silva, J. C. Galzerani, N. T. Moshegov, and P. Basmaji, *Phys. Rev. B* **58**, 10683 (1998).
- ¹⁹A. E. Stephens, D. G. Seiler, J. R. Sybert, and H. J. Mackey, *Phys. Rev. B* **11**, 4999 (1975).